Multivalency-Driven Formation of Te-Based Monolayer Materials: A Combined First-Principles and Experimental study

Zhili Zhu,[1] Xiaolin Cai,[1] Seho Yi,[2] Jinglei Chen,[3] Yawei Dai,[3] Chunyao Niu,[1] Zhengxiao Guo,[4,1] Maohai Xie,[3] Feng Liu,[5] Jun-Hyung Cho,[6,2,1] Yu Jia,[1,*] and Zhenyu Zhang[6,†]

[1]*International Laboratory for Quantum Functional Materials of Henan, and School of Physics and Engineering, Zhengzhou University, Zhengzhou 450001, China*

[2]*Department of Physics, Hanyang University, 17 Haengdang-Dong, Seongdong-Ku, Seoul 133-791, Korea*

[3]*Physics Department, The University of Hong Kong, Pokfulam Road, Hong Kong, China*

[4]*Department of Chemistry, University College London, London WC1E 6BT, United Kingdom*

[5]*Department of Materials Science and Engineering, University of Utah, Salt Lake City, Utah 84112, USA*

[6]*ICQD, Hefei National Laboratory for Physical Sciences at the Microscale, and Synergetic Innovation Center of Quantum Information and Quantum Physics, University of Science and Technology of China, Hefei, Anhui 230026, China*

(Received 25 January 2017; revised manuscript received 19 April 2017; published 5 September 2017)

Contemporary science is witnessing a rapid expansion of the two-dimensional (2D) materials family, each member possessing intriguing emergent properties of fundamental and practical importance. Using the particle-swarm optimization method in combination with first-principles density functional theory calculations, here we predict a new category of 2D monolayers named tellurene, composed of the metalloid element Te, with stable 1T-MoS_2-like (α-Te), and metastable tetragonal (β-Te) and 2H-MoS_2-like (γ-Te) structures. The underlying formation mechanism is inherently rooted in the multivalent nature of Te, with the central-layer Te behaving more metal-like (e.g., Mo), and the two outer layers more semiconductorlike (e.g., S). We also show that the α-Te phase can be spontaneously obtained from the magic thicknesses divisible by three layers truncated along the [001] direction of the trigonal structure of bulk Te, and both the α- and β-Te phases possess electron and hole mobilities much higher than MoS_2. Furthermore, we present preliminary but convincing experimental evidence for the layering behavior of Te on HOPG substrates, and predict the importance of multivalency in the layering behavior of Se. These findings effectively extend the realm of 2D materials to group-VI elements.

DOI: 10.1103/PhysRevLett.119.106101

Two-dimensional (2D) materials have been intensively investigated in recent years for their intriguing emergent properties that can be exploited for various device applications. Many 2D monolayers have been synthesized beyond the first member system of graphene [1–3], including the group-IV monolayers of silicene [4] and stanene [5], the group-V monolayers of black phosphorene [6,7], blue phosphorene [8] and antimonene [9], and the group-III monolayer of borophene [10,11]. Besides these group-III, -IV, and -V elemental monolayers, transition metal dichalcogenides (TMDCs) have also attracted much attention because of their relatively wider, tunable, and direct band gaps and inherently stronger spin-orbit coupling [12,13]. Yet to date, somewhat surprisingly, no prediction or fabrication of group-VI elemental monolayers has been made, whose potential existence would not only further enrich our understanding of the realm of the 2D materials world, but could also offer new application potentials stemming from their unique physical and chemical properties.

In this Letter, we add an attractive new category to the ever increasing 2D materials family by predicting the existence and fabrication of group-VI elemental monolayers centered on the metalloid element Te. Our theoretical calculations reveal that 2D monolayers of Te, named tellurene, can exist in the stable 1T-MoS_2-like (α-Te) structure, as well as the metastable tetragonal (β-Te) and 2H-MoS_2-like (γ-Te) structures. These trilayer arrangements are driven by the inherent multivalency nature of Te, with the central-layer Te behaving more metal-like, and the two outer layers more semiconductorlike. In particular, the monolayer and multilayers of α-Te can be readily obtained via a thickness-dependent structural phase transition from the trigonal bulk Te, with van der Waals-type coupling between neighboring trilayers. Both the α- and β-Te phases possess higher carrier mobilities ranging from hundreds to thousands of $cm^2\,V^{-1}\,s^{-1}$ compared to MoS_2, with significantly enhanced optical absorption properties due to a nearly direct or direct band gap. Furthermore, we present preliminary but convincing experimental evidence for the layering behavior of Te on HOPG substrates, and predict the importance of multivalency in the layering behavior of Se. These findings effectively extend the realm of 2D materials to group-VI elements.

We perform the particle-swarm optimization (PSO) searches [14] in combination with the density-functional theory (DFT) calculations using the Vienna *ab initio* simulation package (VASP) within the projector augmented wave method [15,16]. For the exchange-correlation energy, we employ the PBE functional [17] with the van der Waals

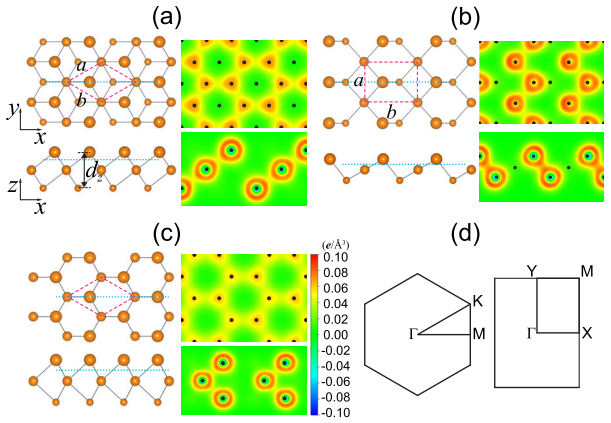

FIG. 1. Top and side views of the optimized structures of tellurene in different phases: (a) α-Te, (b) β-Te, and (c) γ-Te. The surface Brillouin zones for α (or γ) and β phases are drawn in (d). The dashed lines indicate the unit cell of each structure. The total charge density of each structure is plotted at the horizontal and vertical cross sections indicated by the blue dotted lines.

(vdW) correction proposed by Grimme [18] and the screened hybrid functional, HSE06 [19,20]. The kinetic-energy cutoff for the plane wave basis set is chosen to be 500 eV. Te monolayers are modeled by a periodic 1×1 slab geometry with a vacuum thickness of 20 Å. All the atoms are allowed to relax along the calculated forces of less than 0.01 eV/Å. Phonon calculations are performed using larger supercells, as implemented in the Phonopy code [21].

Figure 1 presents the optimized structures of monolayers of tellurene. We identify three different phases denoted by α-, β-, and γ-Te, as shown in Figs. 1(a)–1(c), respectively. The structural parameters and cohesive energy of each optimized structure are listed in Table I. It is seen that α-Te has the 1T-MoS_2-like structure, containing three Te atoms per unit cell. Here, when compared with the 1T-MoS_2 monolayer, there are two distinct types of Te atoms with different coordination numbers (n_c): a central Te atom located at the Mo site has $n_c = 6$, while a Te atom in the upper or lower layer at the S sites has $n_c = 3$. Meanwhile, β-Te is composed of the planar four-membered and chairlike six-membered rings arranged alternately with the lattice constants $a = 4.17$ and $b = 5.49$ Å (see Table I), where a central Te atom has $n_c = 4$, and an upper or lower Te atom has $n_c = 3$. γ-Te has the 2H-MoS_2-like structure, with smaller lattice constants $a = b = 3.92$ Å than those ($a = b = 4.15$ Å) of α-Te. To examine the relative stability of different tellurene allotropes, the cohesive energy (E_c) per atom with respect to the energy of an isolated Te atom is calculated. As shown in Table I, α-Te is energetically the most stable phase, while β-, and γ-Te are the metastable phases.

TABLE I. Structural parameters of tellurene, together with the cohesive energy E_c and charge transfer ΔQ. a and b are the lattice constants, d is the bond length, and d_z is the interval distance between the upper and lower Te layers (see Fig. 1). For comparison, the structural and energetic properties of bulk Te are also listed.

	a, b (Å)	d (Å)	d_z (Å)	E_c (eV/atom)	ΔQ (e)
α-Te	$a = b = 4.15$	3.02	3.67	2.62	0.41
β-Te	$a = 4.17$ $b = 5.49$	3.02 2.75[a]	2.16	2.56	0.11
γ-Te	$a = b = 3.92$	3.08	4.16	2.46	0.29
Te-I	$a = b = 4.33$ $c = 6.05$	2.90	...	2.79	...

[a]Bond length between two Te atoms with $n_c = 3$.

To examine the structural stability of tellurene, we perform the phonon calculations, which can identify the potential presence of soft phonon modes that may lead to structural instability. The calculated phonon spectra of tellurene are displayed in Fig. S1 of the Supplemental Material [22]. We first confirm that all the three phases are thermodynamically stable without imaginary-frequency phonon modes. The dynamic stability is further investigated using *ab initio* molecular dynamics simulations at finite temperatures. We find that the equilibrium structures of α-Te and β-Te hardly change at room temperature, while γ-Te becomes unstable at temperatures above ~200 K. In the movies of the Supplemental Material [22], we illustrate the dynamic stability of each phase at 300 K up to a time period of 3 ps with 1 fs time step.

In Figs. 1(a)–1(c), the total charge densities of α-, β-, and γ-Te reveal their bonding characteristics, respectively. For α- and γ-Te, there exists a metal-ligand-like bonding between the central atom and the outer atoms. On the other hand, for β-Te, the outer atoms with $n_c = 3$ are bonded to each other with the σ bond, while the central atoms interact with the outer atoms in the form of a metal-ligand-like bonding. Consequently, the former bond length (2.75 Å) is much shorter than the latter one (3.02 Å). According to the Bader charge analysis, the charge transfer from the central to the outer atoms amounts to 0.41, 0.11, and 0.29 e in α-, β-, and γ-Te, respectively (see Table I); therefore, the central Te atoms behave more metal-like with a larger n_c, while the outer Te atoms more semiconducting with a smaller n_c. The structural features of tellurene can be further associated with the bonding characters of group-VI elements, where the nonmetallic character is weakened in the order of O > S > Se > Te, leading to a complete metallic character of Po. In particular, Te has the dual characteristics of both metal and nonmetal. It is thus feasible that the two dimensional monolayers of Te can adopt the trilayer atomic structures, e.g., MoS_2-like structure. With the dimensionality reduction, the multivalency-dominated 2D structures with heterogeneous coordination numbers become lower in energy. Collectively, these findings amply reflect the distinct multivalent nature of Te and its vital role in the formation of tellurene.

Figures 2(a)–2(c) show the band structures of α-, β-, and γ-Te, respectively, obtained within the PBE scheme. We find that α- and β-Te are semiconductors with indirect band gaps of $E_g = 0.76$ and 1.17 eV, respectively, while γ-Te is a

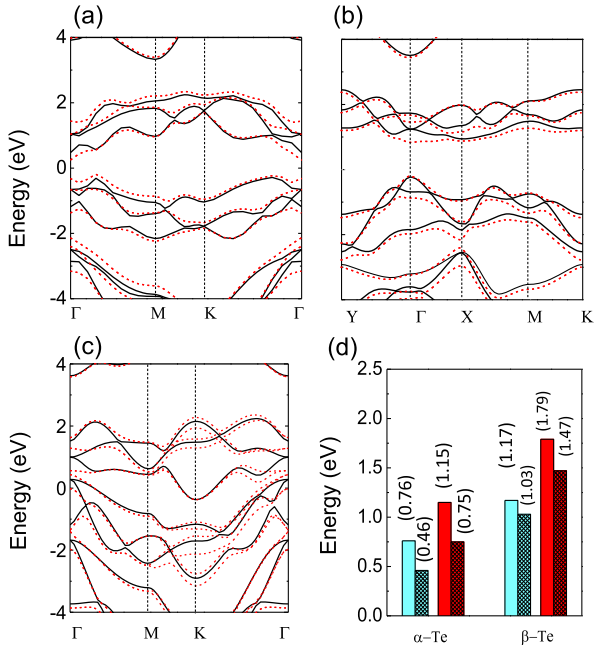

FIG. 2. Band structures of (a) α-Te, (b) β-Te, and (c) γ-Te, obtained within the PBE scheme without (solid) and with (dashed) inclusion of the SOC. (d) Band gaps obtained within the PBE (PBE + SOC) and HSE (HSE + SOC) schemes, as represented by the cyan (cyan meshed) and red (red meshed) bars, respectively.

metal. It is well known that the semilocal PBE scheme may underestimate the band gap. In order to remedy such a potential deficiency in PBE, we perform the hybrid DFT calculations with the HSE06 functional [20,21]. As shown in Fig. 2(d), the HSE calculations for α- and β-Te give increased $E_g = 1.15$ and 1.79 eV, respectively. Given the heavy metal nature of Te, we also examine the effects of SOC on the band structure. The results obtained using within PBE + SOC scheme are plotted with the dashed lines in Figs. 2(a)–2(c). We find that the inclusion of SOC in α- and β-Te induces a transformation from an indirect to a nearly direct and a direct band gap at the Γ point, respectively. This indirect-to-direct band gap change in α- and β-Te may significantly enhance their optical absorbance. Indeed, as seen in Fig. S2, both α- and β-Te exhibit superb optical absorptions, which can be exploited for optoelectronics and photon detection. β-Te also exhibits optical anisotropies, with stronger absorbance along the zigzag chain direction, which can be exploited for developing polarized optical sensors. The HSE + SOC band gap of α-Te becomes 0.75 eV, which is located between the band gaps (~0.7 and ~1.1 eV) of bulk Ge and Si [23], and that of β-Te is 1.47 eV, which is close to that of GaAs.

For potential applications in electronic devices, the newly discovered 2D materials should have high carrier mobilities. To estimate the carrier mobility of tellurene, we calculate their effective masses, which are relatively smaller than those ($m_e^* = 0.47$, and $m_h^* = 0.58\ m_e$) of monolayer 2H-MoS_2 (see Table II). These results suggest that tellurene may possess high electron and hole mobilities. Using the acoustic phonon limited method [24], the room-temperature carrier mobilities of α- and β-Te are found to range from hundreds to thousands of $cm^2\,V^{-1}\,s^{-1}$, much higher than those of monolayer 2H-MoS_2 (see Table II and the Supplemental Material [22]). Here, μ_e and μ_h show large differences in magnitude, indicating asymmetric mobilities of electrons and holes due to their different effective masses. In addition, β-Te has anisotropic characters of electron and hole mobilities along the y direction.

TABLE II. Effective masses m^* and carrier mobilities μ of α-Te, β-Te, and 2H-MoS_2, obtained within the PBE + SOC sheme. For the tetragonal structure of β-Te, the components along the armchair chain (x) and zigzag chain (y) directions are separately given.

	m^* (m_e)		μ (10^3 $cm^2\,V^{-1}\,s^{-1}$)	
	Electron	Hole	Electron	Hole
α-Te	0.11	0.17	2.09	1.76
β-Te	0.83 (x)	0.39 (x)	0.05 (x)	1.98 (x)
	0.19 (y)	0.11 (y)	0.10 (y)	0.45 (y)
2H-MoS_2	0.47	0.58	0.08	0.29

Next we explore possible fabrication route for tellurene and its multilayers. To date, the existing 2D materials can be divided into two categories: those that can be mechanically exfoliated from their layered bulk counterparts, such as graphene and MoS_2; and those, lacking a layered bulk counterpart, that have to be grown epitaxially on proper substrates, such as silicene and stanene. Meanwhile, the trigonal structure of bulk Te (hereafter termed Te-I) has the form of helical chains along the [001] direction, indicating the z direction pointing along the c axis, and the Te films most easily grow in the [001] direction [25], which are qualitatively different from the layering structures of tellurene. But strikingly, monolayer or multilayers of tellurene can be generated via an intriguing new formation mechanism characterized by a thickness-dependent structural phase transition in the ultrathin film regime. We reach this important finding through a systematic study of the Te film stability with increasing film thickness, determined by the formation energy (E_f) as a function of the number of atomic layers, N. Here the initial configurations of the slabs are taken by truncating the bulk Te-I along the [001] direction. The formation energy is given by the cohesive energy difference $E_f = [E_{\rm slab}(N) - NE_{\rm bulk}]/N$, where $E_{\rm slab}(N)$ and $E_{\rm bulk}$ are the total energies of the slab and a single layer in bulk Te, respectively. For these multilayerd systems, we have included the vdW interactions using the DFT-D2 method [18].

Figure 3(a) shows the variations of the formation energy E_f of the fully relaxed Te slabs with increasing N, exhibiting a distinct oscillatory behavior. E_f is referenced to the bulk Te-I structure and positive E_f values indicate

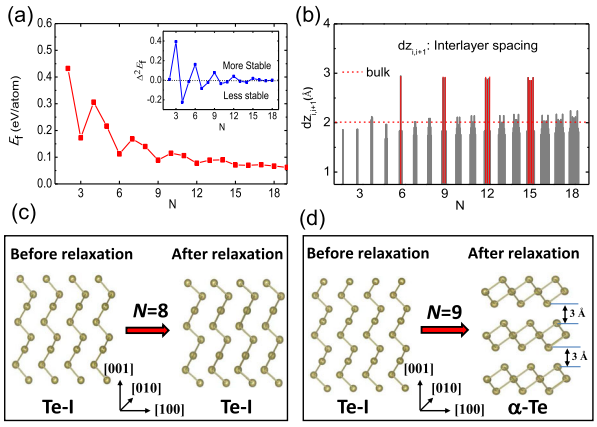

FIG. 3. (a) Formation energies E_f of the fully relaxed Te slabs as a function of the film thickness, with the minima indicating more stable structures. Positive E_f values indicate instability with respect to the bulk Te-I structure.The inset represents the second-order difference of E_f, with positive values indicating more stable systems. (b) Distribution of the layer-resolved interlayer spacing of relaxed Te slabs as a function of the thickness. The dashed line denotes the atomic layer spacing of bulk Te. (c) and (d) The geometric structures of Te slabs at $N = 8$ and 9 before and after structural optimization, respectively, with the corresponding structures marked below.

instability with respect to Te-I (bulk). There are five highly preferred (or magic) thicknesses of $N = 3$, 6, 9, 12, 15 when the thickness of the Te-I slabs increases from $N = 1$ to 20. Strikingly, we find that the Te slabs automatically transform into multilayered structures of α-Te at the magic layer thicknesses, while the Te slabs will keep the chainlike structures of bulk Te away from these magic thicknesses. The inset in Fig. 3(a) highlights the stability of the different slabs by the second difference, while Figs. 3(c) and 3(d) highlight the different structural preferences of Te slabs with $N = 8$ and 9, respectively. We further obtain that the interlayer coupling strength between two neighboring tellurene monolayers (or, equivalently, two Te trilayers) of Te is 26 meV/Å^2, which is on the same order as that of MoS_2 (21 meV/Å^2) [26], suggesting that a single tellurene layer can be readily exfoliated once it is formed.

At present, there is no *a priori* knowledge about which vdW scheme is more accurate for a given system. As cross checks, we also examine the Te film stability as a function of the film thickness with the vdW interactions treated within the widely adopted first-principles-based schemes of Tkatchenko and Scheffler [27] (DFT-TS) and vdW-DF2 [28], respectively. For each scheme, the results qualitatively also support the existence of a structural phase transition from the bulk-truncated Te structure to multilayered tellurene at the identical film thicknesses, but the number of such magic thicknesses is varied depending on the specific version of the vdW scheme. For DFT-TS (vdW-DF2), the layered (or close shelled) structures are found to be highly preferred at the thicknesses of $N = 3$, 6, 9 (3, 6). Here, we note that the optimized lattice parameters of bulk Te obtained using the vdW-DF2 scheme show more severe deviations from the experimental values (see Table S1 of the Supplemental Material [22]), while the DFT-D2 and DFT-TS schemes agree better with experiments. Together, these results convincingly indicate that at least a few monolayers of tellurene will be readily obtained in a typical yet thickness-controlled fabrication approach on a proper substrate favoring layered growth.

To at least partially verify the theoretical predictions of the tellurene structures, we have carried out preliminary experimental studies of Te growth on highly oriented pyrolytic graphite (HOPG) substrates by using molecular beam epitaxy. The experimental details are given in the Sec. S6 of the Supplemental Material [22]. Figure 4(a) shows an STM image of the grown Te film, where the height difference between the consecutive layers amounts to ~4.0 Å (see the height profile in the inset). The atomically resolved STM topographic image of one atomically flat Te film is also displayed in Fig. 4(b), showing a rectangular unit cell of 5.4×4.3 Å^2. The measured step height and unit cell area of the grown Te films match very well with the calculated structural parameters of the β-Te phase [see Fig. 4(c) and Table I].

In contrast to the thickness-dependent structural phase transition mechanism of α-Te, the β-Te phase is the natural consequence of structural relaxation when the bulk helical chain structure is truncated along the equivalent [010] or [100] direction into thin films at proper thicknesses (see Fig. S4 in the Supplemental Material [22] for $N = 3$). We conjecture that the deposited Te atoms highly prefer to initiate their growth in the form of helical chains parallel to the HOPG substrate, and such long chains further evolve into the β-Te phase through relatively mild restructuring. It should be noted that, even though the average formation energy per atom of the α-Te phase is lower than that of the β-Te phase, such thin films reaching the β-Te phase will not

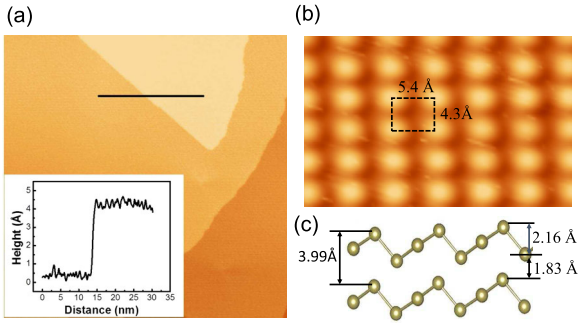

FIG. 4. (a) STM micrograph of an epitaxial Te film grown on HOPG (image size: 75×75 nm^2. Tunneling current: 100 pA, sample bias: 0.6 V). Inset: height profile taken along the black line. (b) Atomically resolved STM image (size: 3.5×2.2 nm^2). The rectangular unit cell is drawn. (c) Side view of a bilayer film in the β-Te phase, showing the calculated monolayer thickness and interlayer spacing.

convert into the α-Te phase, because of a huge kinetic barrier between the two. We anticipate that if Te is grown on a more chemically bounded substrate (but not too strong), the chains may align vertically, and once their lengths are precisely controlled, the α-Te phase is expected to be selected at the magic layer thicknesses divisible by 3.

Finally, the central design principles rooted in multivalency should stimulate active research efforts in searching for other 2D materials consisting of metalloid elements. For instance, we find that 2D monolayers of Se can also exist, but only the 1T-MoS_2-like (α-Se) structure can be stabilized, while the metastable β and γ phases of Te do not have their counterparts in Se [see Fig. S5(a) of the Supplemental Material [22]]. These contrasting behaviors can be attributed to the less metallic nature of Se than Te. However, similar to the Te slabs, the Se slabs are found to transform spontaneously into multilayered structures of α-Se at the magic layer thicknesses of $N = 3$ and 6.

In summary, our the state-of-the-art global structural searching combined with first-principles calculations has resulted in the discovery of a new category of 2D materials composed of the group-VI element of Te. These new 2D materials called tellurene can be stabilized in the MoS_2-like (α-, γ-Te) and tetragonal (β-Te) structures, and their underlying formation mechanism is inherently rooted in the multivalency nature of Te. The α-Te and β-Te monolayers exhibit superb optical absorptions, and possess much higher carrier mobility than MoS_2. The α-Te multilayers can be achieved spontaneously from the bulk truncated films via a novel thickness-dependent structural phase transition. The coupling between neighboring tellurene layers is of vdW type, allowing easy separation of a tellurene layer via mechanical exfoliation. We have presented preliminary but convincing experimental evidence for the layering behavior of Te on HOPG substrates, and further predicted the importance of multivalency in the layering behavior of Se. These findings effectively extend the realm of 2D materials to group-VI elements.

We thank Dr. Xiaoyu Han and Professor Qiang Sun for helpful discussions. This work was partially supported by the NSFC (No. 11274280, No. 11504332, No. 11634011, No. 61434002), the National Basic Research Program of China (No. 2012CB921300 and No. 2014CB921103). Z. X. G. is supported by the UK EPSRC (No. EP/K021192/1). J.-H. C. is supported by the National Research Foundation of Korea (NRF) grant funded by the Korea Government (No. 2015R1A2A2A01003248 and No. 2015M3D1A1070639). F. L. is supported by U.S. DOEBES (No. DE-FG02-04ER46148).

*Corresponding author.
jiayu@zzu.edu.cn
†Corresponding author.
zhangzy@ustc.edu.cn.

[1] K. S. Novoselov, A. K. Geim, S. V. Morozov, D. Jiang, Y. Zhang, S. V. Dubonos, I. V. Grigorieva, and A. A. Firsov, Science **306**, 666 (2004).
[2] C. Berger, Z. Song, X. Li, X. Wu, N. Brown, C. Naud, D. Mayou, T. Li, J. Hass, and A. Marchenkov, Science **312**, 1191 (2006).
[3] A. Castro Neto, F. Guinea, N. Peres, K. Novoselov, and A. Geim, Rev. Mod. Phys. **81**, 109 (2009).
[4] P. Vogt, P. De Padova, C. Quaresima, J. Avila, E. Frantzeskakis, M. C. Asensio, A. Resta, B. Ealet, and G. Le Lay, Phys. Rev. Lett. **108**, 155501 (2012).
[5] F.-f. Zhu, W.-j. Chen, Y. Xu, C.-l. Gao, D.-d. Guan, C.-h. Liu, D. Qian, S.-C. Zhang, and J.-f. Jia, Nat. Mater. **14**, 1020 (2015).
[6] L. Li, Y. Yu, G. J. Ye, Q. Ge, X. Ou, H. Wu, D. Feng, X. H. Chen, and Y. Zhang, Nat. Nanotechnol. **9**, 372 (2014).
[7] H. Liu, A. T. Neal, Z. Zhu, Z. Luo, X. F. Xu, D. Tománek, and P. D. Ye, ACS Nano **8**, 4033 (2014).
[8] Z. Zhu and D. Tománek, Phys. Rev. Lett. **112**, 176802 (2014).
[9] J. P. Ji, X. F. Song, J. Z. Liu, Z. Yan, C. X. Huo, S. L. Zhang, M. Su, L. Liao, W. H. Wang, Z. H. Ni, Y. F. Hao, and H. B. Zeng, Nat. Commun. **7**, 13352 (2016).
[10] A. J. Mannix *et al.*, Science **350**, 1513 (2015).
[11] B. Feng, J. Zhang, Q. Zhong, W. Li, S. Li, H. Li, P. Cheng, S. Meng, L. Chen, and K. Wu, Nat. Chem. **8**, 563 (2016).
[12] B. Radisavljevic, Nat. Nanotechnol. **6**, 147 (2011).
[13] X. D. Xu, W. Yao, D. Xiao, and T. F. Heinz, Nat. Phys. **10**, 343 (2014).
[14] Y. C. Wang, J. Lv, L. Zhu, and Y. M. Ma, Phys. Rev. B **82**, 094116 (2010).
[15] G. Kresse and J. Hafner, Phys. Rev. B **48**, 13115 (1993).
[16] G. Kresse and J. Furthmller, Comput. Mater. Sci. **6**, 15 (1996).
[17] J. P. Perdew, K. Burke, and M. Ernzerhof, Phys. Rev. Lett. **77**, 3865 (1996); **78**, 1396(E) (1997).
[18] S. Grimme, J. Comput. Chem. **27**, 1787 (2006).
[19] J. Heyd, G. E. Scuseria, and Z. Ernzerhof, J. Chem. Phys. **118**, 8207 (2003).
[20] A. V. Krukau, O. A. Vydrov, A. F. Izmaylov, and G. E. Scuseria, J. Chem. Phys. **125**, 224106 (2006).
[21] A. Togo, F. Oba, and I. Tanaka, Phys. Rev. B **78**, 134106 (2008).
[22] See Supplemental Material at http://link.aps.org/supplemental/10.1103/PhysRevLett.119.106101 for details regarding the phonon spectra, molecular dynamics simulations of the structural stability, optical properties, and carrier mobilities of tellurene, as well as related results of Se.
[23] Landolt-Börnstein, *Numerical Data and Functional Relationships in Science and Technology*, edited by O. Madelung, New series Vol. 22a (Springer, New York, 1987), p. 14.
[24] J. S. Qiao, X. H. Kong, Z. X. Hu, F. Yang, and W. Ji, Nat. Commun. **5**, 4475 (2014).
[25] Q. Wang, M. Safdar, K. Xu, M. Mirza, Z. Wang, and J. He, ACS Nano **8**, 7497 (2014).
[26] H. Rydberg, M. Dion, N. Jacobson, E. Schroder, P. Hyldgaard, S. I. Simak, D. C. Langreth, and B. I. Lundqvist, Phys. Rev. Lett. **91**, 126402 (2003).
[27] A. Tkatchenko and M. Scheffler, Phys. Rev. Lett. **102**, 073005 (2009).
[28] K. Lee, E. D. Murray, L. Kong, B. I. Lundqvist, and D. C. Langreth, Phys. Rev. B **82**, 081101 (2010).